Materials Today Bio 32 (2025) 101713

Contents lists available at ScienceDirect

Materials Today Bio

journal homepage: www.journals.elsevier.com/materials-today-bio

Lumbrokinase-containing gelatin nanofibers with multiple bioactivities for effective skin wound healing

Wen-Ling Wang [a,b,c], Yi-Hui Lai [d], Chiung-Hua Huang [e,*], Jui-Yang Lai [f,g,h,i,j,**], Chun-Hsu Yao [d,k,l,***]

[a] School of Post-Baccalaureate Chinese Medicine, College of Chinese Medicine, China Medical University, Taichung, 40402, Taiwan
[b] Department of Chinese Internal Medicine, China Medical University Hospital, Taichung, 40447, Taiwan
[c] Department of Chinese Medicine, China Medical University Hospital Taipei Branch, Taipei, 11449, Taiwan
[d] Department of Biomedical Imaging and Radiological Science, China Medical University, Taichung, 40402, Taiwan
[e] Department of Medical Laboratory Science and Biotechnology, Central Taiwan University of Science and Technology, Taichung, 40601, Taiwan
[f] Department of Biomedical Engineering, Chang Gung University, Taoyuan, 33302, Taiwan
[g] Department of Ophthalmology, Chang Gung Memorial Hospital, Linkou, Taoyuan, 33305, Taiwan
[h] Department of Materials Engineering, Ming Chi University of Technology, New Taipei City, 24301, Taiwan
[i] Center for Drug Research and Development, College of Human Ecology, Chang Gung University of Science and Technology, Taoyuan, 33303, Taiwan
[j] Center for Biomedical Engineering, Chang Gung University, Taoyuan, 33302, Taiwan
[k] School of Chinese Medicine, China Medical University, Taichung, 40402, Taiwan
[l] Department of Bioinformatics and Medical Engineering, Asia University, Taichung, 41354, Taiwan

ARTICLE INFO

Keywords:
Lumbrokinase
Gelatin
Bioactive nanofibrous matrix
Electrospinning
Wound healing

ABSTRACT

Wound healing is a highly complex and intricate biological process involving cellular and molecular events. Given that lumbrokinase is a fibrinolytic enzyme derived from earthworms and exhibits notable anti-inflammatory, anti-fibrotic, and pro-angiogenic functions, this study aims to investigate the development of bioactive gelatin nanofibers containing lumbrokinase (GLK) fabricated through electrospinning as a novel nanomedicine strategy for enhancing wound healing. Our results showed that reducing electrospinning time can increase cross-linking degree and decrease degradation rate to maintain an effective concentration of released LK for supporting long-term biological processes. Cells cultured with biocompatible GLK displayed good adhesion and extensive spreading, increased VEGF production, and lowered IL-6 and TNF-α secretion. The GLK with superior and multiple bioactivities was further tested for tissue regeneration potential in a rat model of skin defect. The treatment of animals with GLK shortens wound healing time, reduces damage caused by inflammation, and increases collagen production, angiogenesis, and fibroblast proliferation/epithelialization, demonstrating that the healing effect on the local wounds is comparable to that of Comfeel group. Overall, the findings from preclinical studies suggest high promise of the LK-loaded biopolymer nanofibers as bioactive dressing materials for promoting a regenerative environment and accelerating wound healing, indicating its future translational potential.

1. Introduction

The skin is the largest organ in the human body and is crucial in maintaining homeostasis [1]. Skin injuries, which arise from several causes, including trauma, burns, surgical procedures, and chronic diseases, can have significant consequences, such as infections and loss of functional integrity. The wound healing usually progresses through three phases: inflammatory, proliferative, and remodeling [2]. The intricate nature of the healing process poses substantial challenges to the development of effective therapeutics for wound treatment. Natural products are promising therapeutic agents for wound healing. One such intriguing candidate is earthworm extract, which has been used in traditional medicine for centuries. In Chinese medicine, *Lumbricus* spp., also known as earthworms, are used to treat various conditions,

* Corresponding author.
** Corresponding author. Department of Biomedical Engineering, Chang Gung University, Taoyuan, 33302, Taiwan.
*** Corresponding author. Department of Biomedical Imaging and Radiological Science, China Medical University, Taichung, 40402, Taiwan.
E-mail addresses: chhuang@ctust.edu.tw (C.-H. Huang), jylai@mail.cgu.edu.tw (J.-Y. Lai), chyao@mail.cmu.edu.tw (C.-H. Yao).

https://doi.org/10.1016/j.mtbio.2025.101713
Received 23 January 2025; Received in revised form 18 March 2025; Accepted 27 March 2025
Available online 28 March 2025

including burns, arthritis, itching, and inflammation [3–8].

A component within earthworm extract that is of particular interest is lumbrokinase (LK), which has been identified as a bioactive proteolytic enzyme. It disintegrates fibrin, which is a protein that forms clots within blood vessels [9]. Additionally, LK exhibits notable anti-inflammatory, antioxidative, antifibrotic, antimicrobial, and anticancer properties [10–12]. Clinically, LK is primarily used for thrombotic diseases, including ischemic cerebrovascular and cardiovascular conditions, platelet aggregation disorders, deep vein thrombosis, and lipid metabolism abnormalities associated with nephrotic syndrome. Furthermore, earlier observations have indicated that LK possesses intrinsic wound healing properties [13]. Hence, this study explored the potential of an innovative LK-based wound dressing material.

Nanofiber dressings have emerged as a promising technology for wound healing. These nanofibrous membranes, which are composed of biocompatible polymers, are designed to mimic the intricate structure of the skin's natural extracellular matrix (ECM) [14]. One of the key advantages of electrospun nanofibers for wound healing application is their ability to closely resemble the ECM, providing essential structural support for cell adhesion, migration, and proliferation, and facilitating the remodeling and neo-tissue formation [15–18]. Furthermore, the high porosity of electrospun nanofiber-based scaffolds has been demonstrated to facilitate nutrient diffusion and metabolic waste removal, both of which are crucial for cellular function and tissue regeneration. However, despite these advantages, electrospinning may have lower production efficiency compared to some other fiber-generating techniques like melt, dry, or wet spinning.Among the various materials used in nanofiber wound dressings, gelatin is a highly biocompatible and biodegradable protein derived from collagen with extensive biomedical applications. The incorporation of gelatin into electrospun nanofiber membranes further enhances their suitability for wound healing, as these membranes are easily degradable and resorbable by the body, making them highly favorable for clinical applications. Their simple and cost-effective manufacturing process further promotes them as potential wound dressings and tissue-engineered membranes [19–21].

In the present study, we focus on the development of LK-loaded gelatin nanofiber membranes using electrospinning. Rigorous characterization through comprehensive morphological and physicochemical analyses is performed to evaluate the structural and functional properties of the membranes. Furthermore, the wound-healing effects of these membranes are investigated through a series of assays, including cytocompatibility, cell migration, blood tube formation, anti-inflammatory effects, wound healing, and in-vitro/in-vivo animal models. The promising results obtained from these investigations substantiate the potential of LK-loaded gelatin nanofiber membranes as effective therapeutic agents for wound healing.

2. Experimental

2.1. Materials and cell lines

Type A gelatin from porcine skin was purchased from Sigma (St. Louis, MO, USA). Poly(vinyl) alcohol (PVA) (MW = 1400) was supplied by SHOWA (Tokyo, Japan). All cell culture reagents were purchased from Invitrogen. Lumbrokinase was supplied by NOVA Pharma and Liposome Biotech Co (Kaohsiung, Taiwan). Mouse fibroblast cells (L929) were cultured in a medium with DMEM with 2 mM Glutamine + 10 % Fetal Bovine Serum (FBS). Human umbilical vein endothelial cells (HUVECs) were cultured in a medium with Earles' salts and FBS but without a growth factor. The osteoclasts murine monocyte/macrophage RAW 264.7 cells (BCRC no. 60001, Food Industry Research and Development Institute were cultured in a growth medium of DMEM with 5 % FBS and 1 % penicillin/streptomycin (Gibco). All cell lines were grown at 37 °C under 5 % CO_2 in the air.

2.2. Bioactive assay of lumbrokinase

2.2.1. Cell cytotoxicity assay

L929 (5×10^3 cells/well), HUVECs (1×10^4 cells/well), and RAW 264.7 cells (5×10^3 cells/well) were used to determine the cytotoxicity of LK. Cells were cultured in triplicate with the culture medium with different concentrations of LK in 48-well, flat-bottomed tissue culture plates for 2 days at 37 °C under 5 % CO_2 in the air, and cell viability was determined via an MTT assay.

2.2.2. Two–dimensional cell migration assay

L929 were seeded at the density of 1×10^5 cells per well in the ibidi Culture-Insert a Well for the wound healing assay and incubated at 37 °C for 24 h. After removing the Culture-Inserts, the cells were cultured in the culture medium with various concentrations of LK for 4 h. Cell migration was monitored by inverse microscopy and analyzed by ImageJ. The ratio of wound area (%) was calculated as At/Ai × 100 %, where Ai is the initial area of the scratch circle, and At is the transparent area after culturing for a given length of time.

2.2.3. Tube formation assay

The μ-Slide angiogenesis (ibidi) is applied for tube formation assay. 10 ml of Matrigel (Corning® BioCoat™) was coating onto every inner wells and polymerized at 37 °C for 30 min. Then, HUVEC cells suspended in a culture medium with different concentrations of LK at the density of 5×10^3 were added to each well after 4-h culturing. The Wimasis image analysis quantified the tube formation. The in vitro tube formation studies blood vessel development by measuring the angiogenesis stage of endothelial cell reorganization to form capillary-like structures.

2.2.4. Anti-inflammatory assay

RAW 264.7 were seeded at a density of 2×10^4 cells per well in the culture medium with 1 μg/ml Lipopolysaccharide (LPS) and various concentrations of LK for 2 days. Interleukin 6 (IL-6) and tumor necrosis factor-α (TNF-α) assays were performed using commercially available enzyme-linked immunosorbent assay (ELISA, Abcam). The concentration of IL-6 and TNF-α were calculated regarding a standard curve constructed using the recombinant cytokine provided with each kit.

2.3. Preparation and characterization of gelatin nanofiber containing lumbrokinase (GLK)

2.3.1. Preparation of GLK membranes

The gelatin mixtures were dissolved in formic acid (85 wt %) at a concentration of 17 wt %. An aqueous solution of PVA (10 wt %) was then added to the gelatin (GEL) solution at a GEL/PVA ratio of 9/1 (v/v). The solution was agitated at room temperature for 1 h before electrospinning the gelatin onto the HERADERM PU film. Next, the LK was added to the GEL/PVA solution at the final 20 μg/ml concentration. As guided by our earlier works [22–24], the tip-to-collector distance was 10 cm, the electric potential was maintained at 20 kV. In this study, the flow rate was controlled at 0.1, 0.4, and 0.8 ml/h. After 1-h and 2-h electrospinning, the gelatin membranes were cross-linked in 50 wt% glutaraldehyde vapor for 45 min. The prepared membranes were sterilized overnight with ultraviolet (UV) rays and placed on 24-well polystyrene tissue culture plates.

2.3.2. Fourier transform infrared spectroscopy

The gelatin membrane composition was analyzed using Fourier transform infrared spectroscopy (FTIR, Spectrum Two, PerkinElmer) in the 4000–400 cm^{-1} range using KBr pellets.

2.3.3. Microscopic morphological observation

Dry membranes were coated with a gold layer and examined via scanning electron microscopy (SEM, Hitachi S3000V, Japan).

Histograms of the fiber diameters were generated from the SEM.

2.3.4. Swelling ratio measurements

The nanofibers were placed in 24-well plates and flattened with an O-ring. One ml of double distilled water (ddH_2O) was added to each sample and incubated for 0, 3, 6, 12, 24, and 48 h. The diameter variations determined the swelling ratios of the nanofibers.

2.3.5. Degradation assay

One milliliter of distilled 1X PBS was added to each weighed membrane sample, and the samples were then incubated for 1, 4, 7, and 14 days. Each sample was removed and gently blotted with filter paper. Then, the sample was lyophilized and weighed. The weight loss (%) was calculated as (Wi–Wd)/Wi × 100 %, where Wi is the initial weight of the specimen in its dry state, and Wd is the weight of the specimen in its dry state after submersion in distilled 1X PBS for a given length of time.

2.3.6. Evaluation of the cross-linking index

A ninhydrin assay was used to evaluate the cross-linking degree of the electrospun gelatin nanofibers. The amount of the free amino groups in the gelatin nanofibers was determined using the ninhydrin (2,2-dihydroxy-,3-indanedione) assay. Three mg of nanofibers were soaked in distilled water and heated with ninhydrin reagent for 20 min. After the solution was cooled to room temperature and diluted with 50 % isopropyl alcohol, the optical absorbance of the solution was recorded using a spectrophotometer (ELISA reader, Model Genesys™ 10, Spectronic Unicam, New York, USA) at 570 nm (wavelength of the blue-purple color) using glycine at various known concentrations as the standard [25]. The amount of free amino grouping in the original (Ci) and residual gelatin (Cf) is proportional to the optical absorbance of the solution. The cross-linking index was calculated as the cross-linking index (%) = (Ci-Cf)/Ci × 100 %.

2.3.7. Drug release assay

One-milligram samples of the GLK membranes of 1-h or 2-h electrospinning were each soaked in 1 ml of distilled water for 0.5, 1, 1.5, 3, 6, 12, 24, and 48 h. Each sample was then analyzed via an indirect ELISA assay kit purchased from Bioss.

2.4. In vitro analysis of L929 cells co-culture with GLK membranes

2.4.1. In vitro cytocompatibility, collagen, and matrix metalloproteinase −1 (MMP-1) assay

The prepared membranes (15 mm^2 diameter) were sterilized overnight with ultraviolet (UV) rays and placed on 24-well polystyrene tissue culture plates. L929 cells were cultured in triplicate at a density of 1 × 10^4 cells/well in 24-well, at 37 °C for 2 days. After removing the culture medium, the cell viability was determined via an MTT assay. Then, the culture medium was centrifuged at 2000 g for 10 min, and Collagen type I (Abcam) and MMP-1 (MyBioSource)were quantitated using ELISA kits.

2.4.2. Immunohistochemical analysis

GLK membranes were electrospun for 1 h on a coverslip and sterilized by UV for 24 h. L929 cells were then co-cultured with the coverslip for 24 h. The electrospun membranes seeded with L929 cells were rinsed with phosphate-buffered saline and fixed with 4 % formaldehyde for 15 min at room temperature. For quantitative analysis, the nanofibrous membranes were then counterstained with 4',6-diamidino-2-phenylindole (DAPI, 1:5000; Invitrogen). For the immunohistochemical assay, the nanofibrous gelatin-coated coverslips were probed with anti-β-actin antibodies (1:1000) and labeled with goat anti-mouse antibodies (1:200). The samples were then sealed and examined using confocal microscopy (Leica *Microsystems, Wetzlar, Germany)*.

2.5. In vitro analysis of HUVEC cells co-culture with GLK membrane

2.5.1. In vitro cytocompatibility and VEGF assay

The prepared membranes (15 mm^2 diameter) were sterilized overnight with ultraviolet (UV) rays and placed on 24-well polystyrene tissue culture plates. HUVEC cells were cultured in triplicate at a density of 2 × 10^4 cells/well in 24-well, at 37 °C for 2 days. After removing the culture medium, the cell viability was determined via an MTT assay. Then, the culture medium was centrifuged at 2000 g for 10 min, and VEGF was quantitated using ELISA kits (Abcam).

2.5.2. Three-dimensional cell migration assay

The membranes were placed in the lower well, and M199 medium with 10 % FBS was added to each lower well. Each upper well has 5 × 10^3 HUVECs in 140 μL serum-free culture medium. The membrane in the upper well contacted the bottom well solution, which was incubated at 37 °C for 24 h. After removing the upper well, the cells were incubated for 24 h for attachment. The cells were stained with hematoxylin, and cell number was counted under microscopic observation.

2.6. In vitro analysis of RAW 264.7 cells co-culture with GLK membrane

2.6.1. In vitro cytocompatibility assay

The prepared membranes (15 mm^2 diameter) were sterilized overnight with ultraviolet (UV) rays and placed on 24-well polystyrene tissue culture plates. RAW 264.7 cells were cultured in triplicate at 1 × 10^4 cells/well density in 24-well, at 37 °C for 2 days. After removing the culture medium, the cell viability was determined via an MTT assay.

2.6.2. In vitro anti-inflammatory assay

RAW 264.7 cells were cultured in triplicate at 2 × 10^4 cells/well density and treated with 1 μg/ml LPS for 2 days. The culture medium was centrifuged at 2000 g for 10 min, and IL-6 and TNF-α were quantitated using ELISA kits.

2.7. Wound healing assay in an animal model

2.7.1. In vivo animal evaluation

Male Sprague-Dawley (SD) rats weighing 350–400 g were used and treated according to the Ethical Guidelines of the Animal Center at China Medical University (CMU). The animal use protocol (protocol ID: CMUIACUC-2017-253) was approved by CMU's Institutional Animal Care and Use Committee (IACUC). In this study, a total of 48 rats ($n = 12$ per group) were used and divided into one control (untreated) group and three experimental groups: the Comfeel® (i.e., hydrocolloid-based wound dressings primarily composed of sodium carboxymethylcellulose, elastomers, and adhesives, designed to maintain a moist wound environment that promotes healing [26]) group, the G1 group, and the GLK1 group.

2.7.2. Wound-healing measurement in rats

The hair (5 × 8 cm^2) on the back of each rat under anesthesia with ether was removed using a hair remover. After removing four areas (15 × 15 mm^2) of skin, the wound surfaces were disinfected with I_2. Next, various membranes (15 × 15 mm^2) were placed on the wound surfaces, which were subsequently bounded with the sterile gauze. Following 7, 14, and 21 days, the recovery ratio was calculated as (Ai–Au)/Ai × 100 %, where Ai is the initial area of the wound and Au is the area of the unrecovered wound surface.

2.7.3. Histopathological studies

Skin specimens were fixed in 10 % buffered formalin for hematoxylin and eosin (HE) staining, and the skin specimens were fixed in Bouin's solution for Masson's trichrome (MT) staining. All skin specimens were viewed under a light microscope to evaluate collagen formation and wound-healing processes.

2.7.4. Collagen assay in wound area

Skin samples from the wound area were dried and ground into powder. Ten percent pepsin was mixed with the skin sample powder and incubated at 4 °C overnight for protein extraction. A QuickZyme collagen assay kit was applied for collagen quantitation.

2.7.5. Quantitation of blood vessels and follicles in the wound area

Skin samples for blood vessel staining (von Willebrand factor, vWF) staining were fixed in normal 10 % buffered formalin. Blood vessel and follicle numbers were counted in 0.15 cm^2 specimens.

2.8. Statistical analysis

The results are presented as the mean standard deviation. Statistical analysis was conducted using Student's *t*-test or one-way analysis of variance followed by a *post hoc* Fisher's least significant difference test for multiple comparisons. Levels of statistical significance were set at $p < 0.05$.

3. Results and discussion

3.1. In-vitro bioactive assay of LK

3.1.1. LK increased cell proliferation

The effect of LK on cell viability was assessed using the MTT assay. LK concentrations below 100 μg/mL did not exhibit any toxic effects on L929 fibroblasts, human umbilical vein endothelial cells (HUVECs), and Raw 264.7 macrophages (Fig. 1). Furthermore, LK demonstrated the ability to enhance the proliferation of L929 cells within the range of 0.0001–0.1 μg/mL and promote the proliferation of HUVECs within the range of 0.01 and 100 μg/mL. However, LK did not demonstrate the ability to enhance the proliferation of RAW 264.7 macrophages within the range of 0.0001–0.1 μg/mL (Fig. 1).

3.1.2. LK accelerated the two-dimensional (2D) migration of L929 cells

The wound-healing assay is a widely used laboratory technique employed to investigate the collective migration of cells in a 2D setting. To initiate the assay, a gap was deliberately formed using the Ibidi culture system. Subsequently, the L929 cells were introduced into the wells and cultured for 24 h, followed by exposure to various concentrations of LK (Fig. 2A). Notably, LK at a concentration of 0.1 μg/mL exhibited the highest efficacy in promoting the migration of L929 cells. This concentration significantly reduced the initial gap area by approximately 26 % (Fig. 2A).

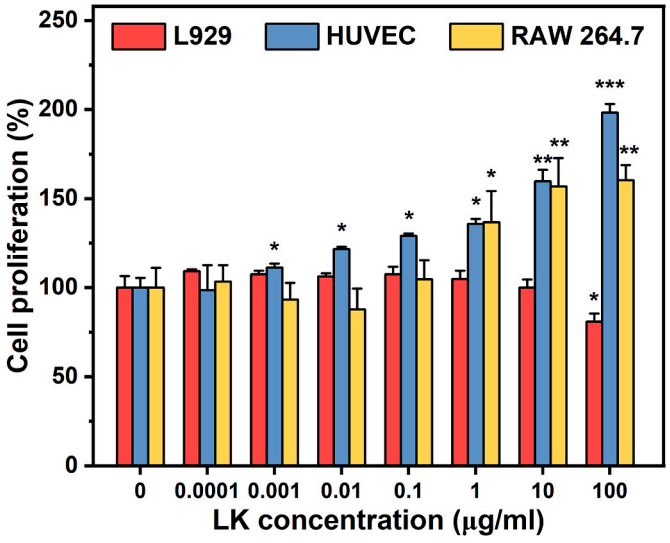

Fig. 1. Bar graph illustrates the cell viability of L929, HUVEC, and RAW 264.7 after a 2-day culture with various concentrations of lumbrokinase. Asterisks indicate statistically significant differences (*$p < 0.05$; **$p < 0.01$; ***$p < 0.001$) as compared with the group of 0 μg/ml LK.

3.1.3. LK promoted angiogenesis in HUVECs

Tube-formation assay is a rapid and quantitative method used to evaluate the effect of a substance on angiogenesis and the formation of new blood vessels. As shown in Fig. 2B, HUVECs were cultured on Matrigel and exposed to various LK concentrations. Remarkably, when the HUVECs were treated with LK concentrations ranging from 0.1 to 10 μg/mL, they exhibited enhanced ability to form cell–cell networks, thus resulting in increased tube formation compared with that in the control group. Several vital parameters were measured to comprehensively analyze the dose-response relationship of LK-induced HUVEC tube formation, including the cell coverage area, total tube length, branch points, loop number, and vessel number (Fig. S1). Notably, at a concentration of 0.1 μg/mL, LK substantially increased the cell coverage area by 72.3 % (Fig. S1A), the total tube length by 40.7 % (Fig. S1B), the number of branch points by 50 % (Fig. S1C), the loop number by 187.5 % (Fig. S1D), and the vessel number by 33.4 % (Fig. S1E). The effects of 0.1 μg/mL LK on angiogenesis were similar to those of higher LK concentrations (1 and 10 μg/mL), as indicated by the results, which were similar to those of the control group. These findings suggest that even at relatively low concentrations, LK possesses significant angiogenic properties and can effectively induce the formation of HUVEC tube networks.

3.1.4. LK exhibited prominent anti-inflammatory effects

The anti-inflammatory properties of LK were evaluated by examining the production of IL-6 and TNF-α in RAW 264.7 macrophages. Following stimulation with lipopolysaccharide, RAW 264.7 cells were treated with varying concentrations of LK. The results revealed that LK at a concentration of 0.1 μg/mL reduced IL-6 production by 26.53 % (Fig. 2C) and TNF-α production by 24.14 % (Fig. 2C). These findings indicate that 0.1 μg/mL of LK exhibit significant anti-inflammatory effects in RAW 264.7 macrophages. Furthermore, LK at a concentration of 0.1 μg/mL demonstrated no cytotoxicity toward L929 fibroblasts, HUVECs, and RAW 264.7 macrophages. Additionally, this concentration of LK promoted cell proliferation and tube formation, as well as exerted anti-inflammatory effects. Consequently, 0.1 μg/mL was selected as the optimal concentration of LK for subsequent investigations, as it yielded favorable biological effects without causing harm to the cells under investigation.

3.2. Electrospinning and parameter optimization for GLK membranes

3.2.1. Flow rate

The flow rate is crucial in determining the diameters of the nanofibers during electrospinning. In this study, gelatin nanofibers incorporating LK were electrospun with a tip-to-collector distance of 10 cm and an electric potential of 20 kV. The flow rates used were 0.1, 0.4, and 0.8 mL/h. The morphology of the GLK nanofibers was observed using scanning electron microscopy (SEM) (Fig. 3A). Interestingly, regardless of the flow rate, the average fiber size was consistently ~100 nm (Table S1). At low flow rates (0.1–0.4 mL/h), the electrospun fibers appeared cylindrical and exhibited a uniform structure. However, when the flow rate was increased to 0.8 mL/h, beaded fibers were formed. Therefore, after considering manufacturing efficiency, a flow rate of 0.4 mL/h was determined to be the optimal electrospinning condition for GLK. This flow rate yielded uniform cylindrical fibers, which are desirable for further applications.

3.2.2. Fabrication time

To investigate the effect of fabrication time on the physical properties and drug release rate of the nanofibers, two types of gelatin membranes containing LK were electrospun for different durations: 1 h

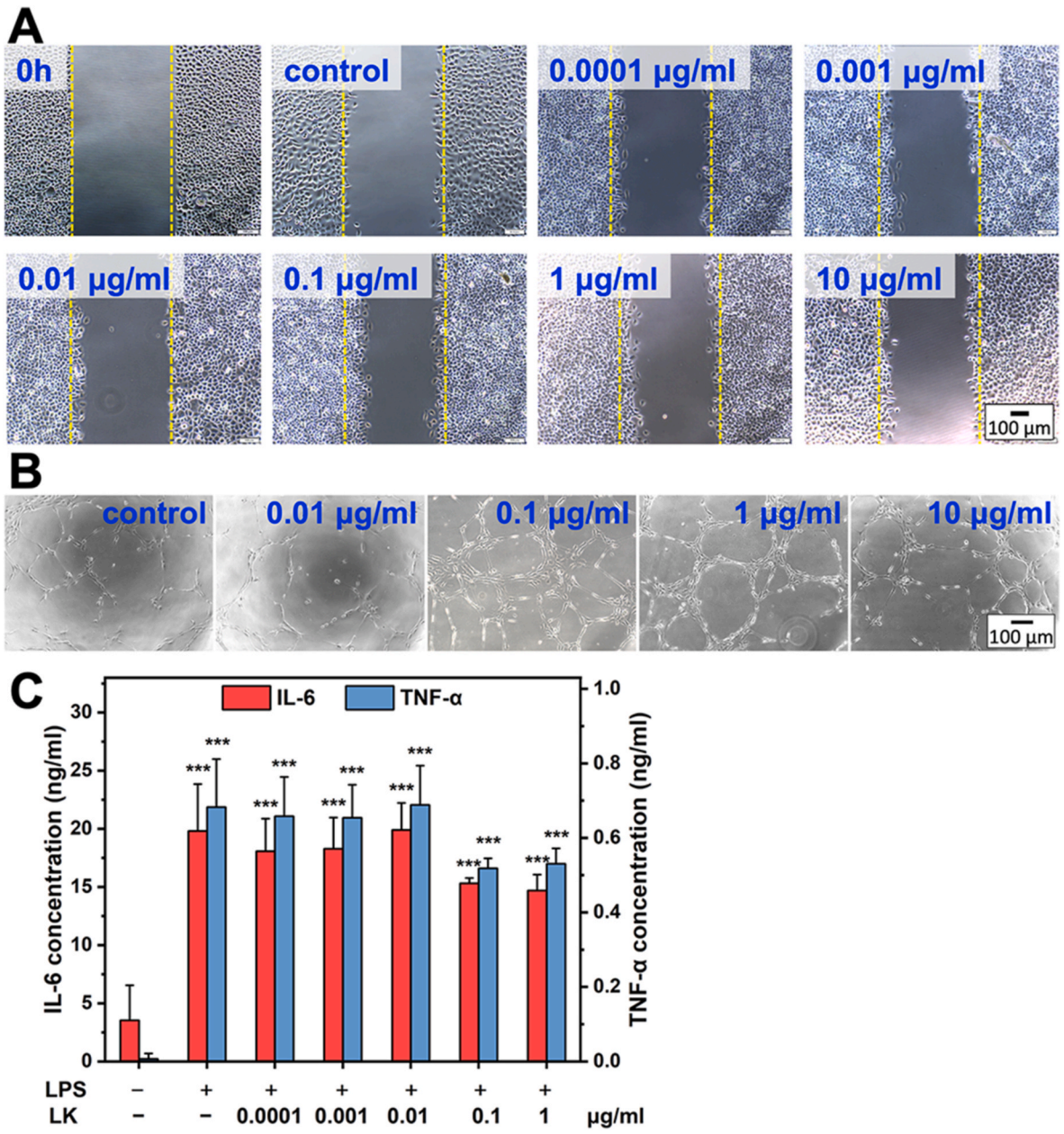

Fig. 2. Effects of LK on wound-healing, angiogenesis, and anti-inflammation. (A) A two-dimensional cell migration (wound–healing) assay was performed using L929 cells cultured with various concentrations of LK for 4 h. A representative image of six experiments is shown for each group. (B) The effect of LK on in vitro angiogenesis was evaluated with a HUVEC tube formation assay. The tube formation after treatment with different concentrations of LK was microscopically compared. (C) The effect of LK on anti-inflammation was evaluated with ELISA assay. IL-6 and TNF-α production were measured by ELISA assay. RAW 264.7 macrophages were cultured with 1 μg/ml LPS and different concentrations of LK for 2 days. Asterisks indicate statistically significant differences (***$p < 0.001$) as compared with the group of 0 μg/ml LK.

(GLK1) and 2 h (GLK2). The addition of LK did not appear to alter the properties of the gelatin nanofibers, as confirmed via FTIR analysis. The FTIR spectra of the G1 and GLK1 membranes exhibited similar absorption peaks (Fig. S2); this suggests that the incorporation of LK did not significantly affect the molecular structure of the gelatin nanofibers.

In the 48-h swelling ratio assay, GLK1 exhibited a maximum swelling ratio of 51.7 %, whereas, GLK2 exhibited 96.6 % (Fig. 3B). Moreover, after 14 d of soaking, the degradation rates of GLK1 and GLK2 were 48 ± 1.5 % and 57 ± 2.7 %, respectively (Fig. 3C). As compared to GLK1, GLK2 had larger swelling ratio, which is primarily attributed to high water absorption capacity of the membrane with a lower cross-linking density. This result was confirmed via a ninhydrin assay, which revealed that GLK2 possessed a lower cross-linking degree (Fig. 3D), thus resulting in increased swelling and degradation rates. The degradation rate significantly affected the drug-release efficiency. Therefore, an indirect enzyme-linked immunosorbent assay (ELISA) was employed to assess the drug release over 14 d. LK was mixed directly with the polymer solution prior to electrospinning, and cross-linking was performed on the resulting nanofibers. The total drug loading content was 20 μg per sample. As LK was incorporated before cross-linking, the cross-linking duration did not affect the drug-loading content. After 24 h of soaking, the LK release concentrations from GLK1 and GLK2 were measured to be 0.75 and 2.89 μg/mL, respectively. Over 14 d, the cumulative release concentrations of LK from GLK1 and GLK2 were 0.75–1.2 and 2.89–5.88 μg/mL, respectively (Fig. 3E).

Based on the in-vitro results, LK concentrations within the range of

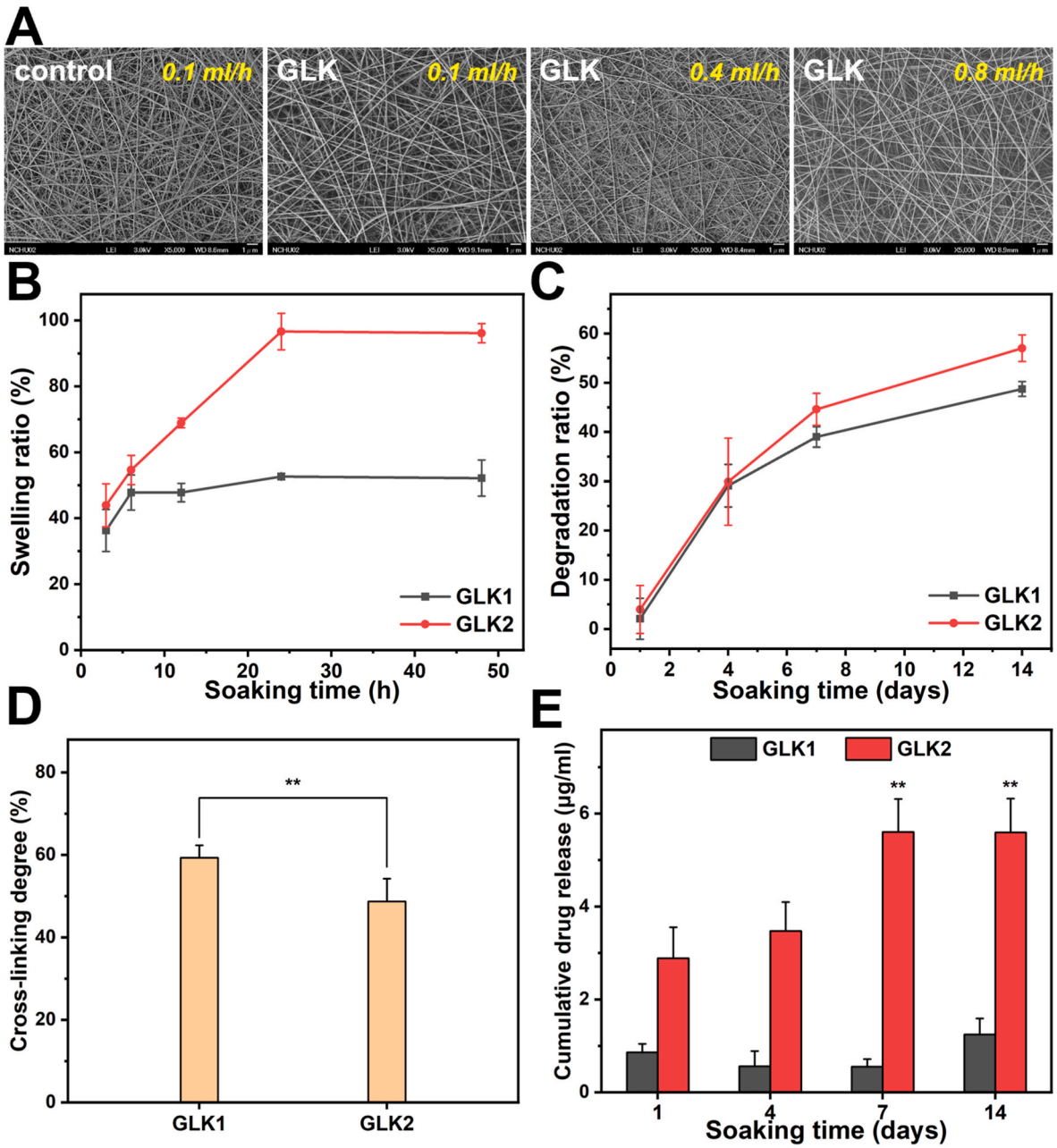

Fig. 3. Characterization of GLK membranes. (A) Scanning electron microscopy (SEM) images of electrospun GLK membranes. The control represents gelatin nanofiber electrospun morphology at a 0.1 ml/h flow rate. The morphology of GLK membranes electrospun at flow rates of 0.1, 0.4, and 0.8 ml/h. Bars: 1 μm. (B) swelling ratio, (C) degradation rate, (D) cross-linking degree, and (E) cumulative drug release profile of GLK1 and GLK2 membranes. Asterisks indicate statistically significant differences (**$p < 0.01$) as compared with the group of 1 day.

0.1–1 μg/mL performed favorably in terms of 2D migration, tube formation, and anti-inflammatory assays. Additionally, the drug-release assay results demonstrated that the GLK membranes fabricated for 1 and 2 h released effective drug concentrations. Therefore, further investigations were conducted to determine the optimal fabrication time for the GLK1 and GLK2 membranes.

3.3. In-vitro cytocompatibility and functional analyses of GLK1 and GLK2 membranes

3.3.1. GLK membranes exhibit good cytocompatibility

Following a 2-D co-culture of L929 cells with GLK1 and GLK2, the cytocompatibility of these materials was assessed using the MTT assay. The results confirmed that GLK1 and GLK2 exhibited cytocompatibility toward L929 cells. Notably, GLK1 substantially promoted L929 cell proliferation (by up to 100 %). This increase was greater than that observed for GLK2 (Fig. 4A).

3.3.2. GLK1 membranes increase the production of type-I collagen and matrix metalloproteinase 1 (MMP-1)

All tested membranes, including gelatin membranes electrospun for 1 h (G1), 2 h (G2), GLK1, and GLK2, stimulated type-I collagen production in co-cultured L929 cells. Notably, L929 cells co-cultured with GLK1 exhibited a remarkable 12-fold increase in type-I collagen production compared with that in the control group (Fig. 4B). The levels of MMP-1 in the supernatants were assessed using an ELISA. As shown in Fig. 4B, GLK1 and GLK2 reduced MMP-1 production by 15.2 % and 18.4 %, respectively. Consequently, GLK1 outperformed GLK2 in most in-

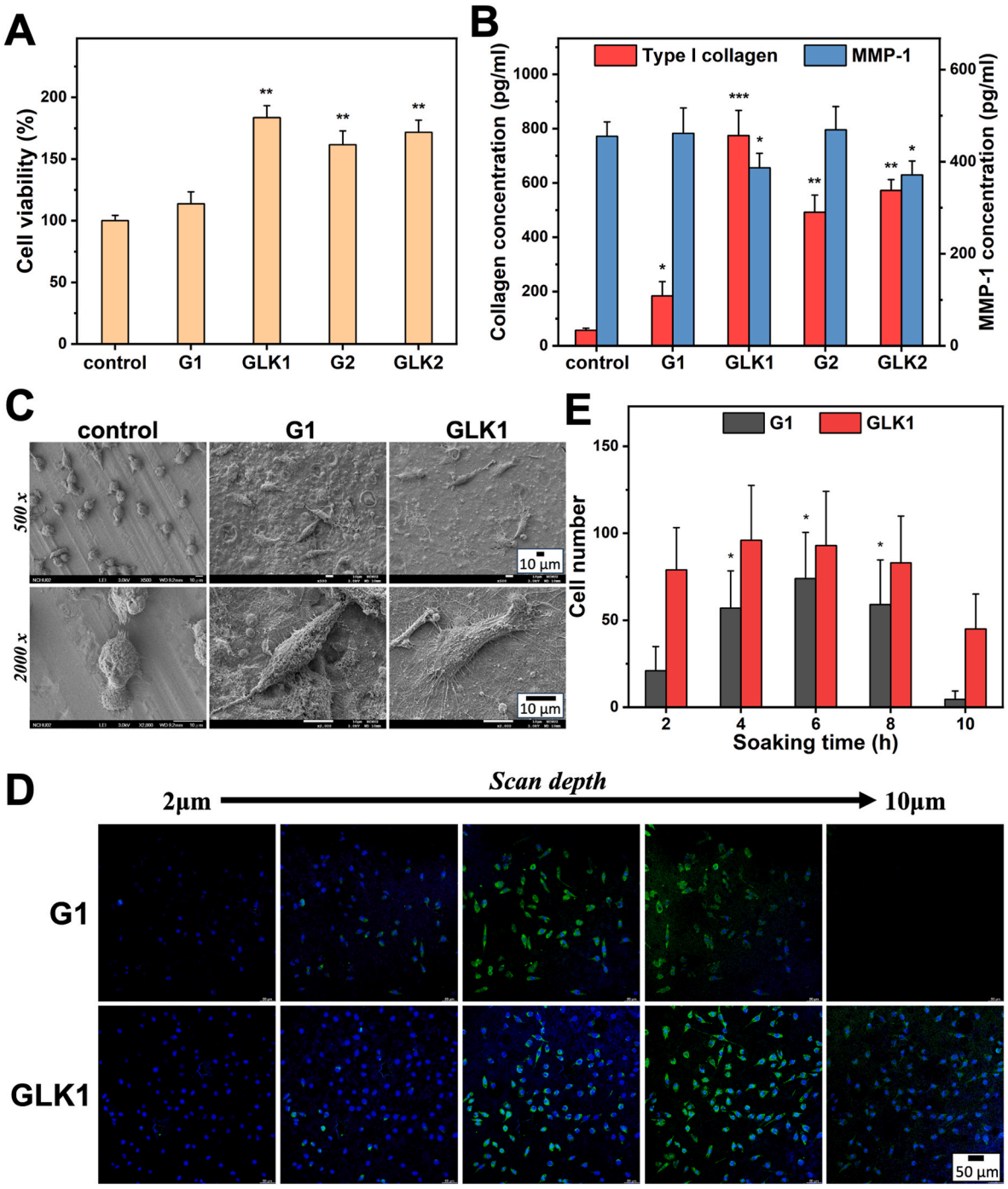

Fig. 4. Comparison of bioactive effects of G1 and GLK membranes co-cultured with L929 cells. Bar graphs illustrate the outcomes of L929 cell viability (A), type I collagen production, and MMP-1 production (B) after a 2-day co-culture with different membranes. Asterisks indicate statistically significant differences (*$p <$ 0.05; **$p < 0.01$; ***$p < 0.001$) as compared with control group. (C) The SEM morphology of the L929 cells cultured with control, G1, and GLK1 membranes at 37 °C for 6 h. Bars: 10 μm. (D) Immunohistochemical staining was performed on L929 cells seeded and grown on G1 and GLK1 membranes for 24 h. The membranes (green) were probed with anti-β-actin antibodies and labeled with goat anti-mouse FITC antibodies. L929 cells were then counterstained with DAPI for quantitative analysis (blue). (E) The quantitative comparison of cell numbers at different depths in the G1 and GLK1 membranes. Asterisks indicate statistically significant differences (*$p < 0.05$) as compared with the group of 2 h. (For interpretation of the references to color in this figure legend, the reader is referred to the Web version of this article.)

vitro bioactive assays. Therefore, GLK1 was selected for subsequent studies as it exhibited more favorable outcomes with respect to increased type-I collagen production and decreased MMP-1 levels.

3.4. In-vitro assays of cells co-cultured with GLK1 membrane

3.4.1. GLK1 membrane supported L929 cell adhesion

Fig. 5A presents the SEM images of L929 cells co-cultured with control, G1, and GLK1 membranes. The control group exhibited round fibroblasts with unsatisfactory attachment, thus indicating a reduced

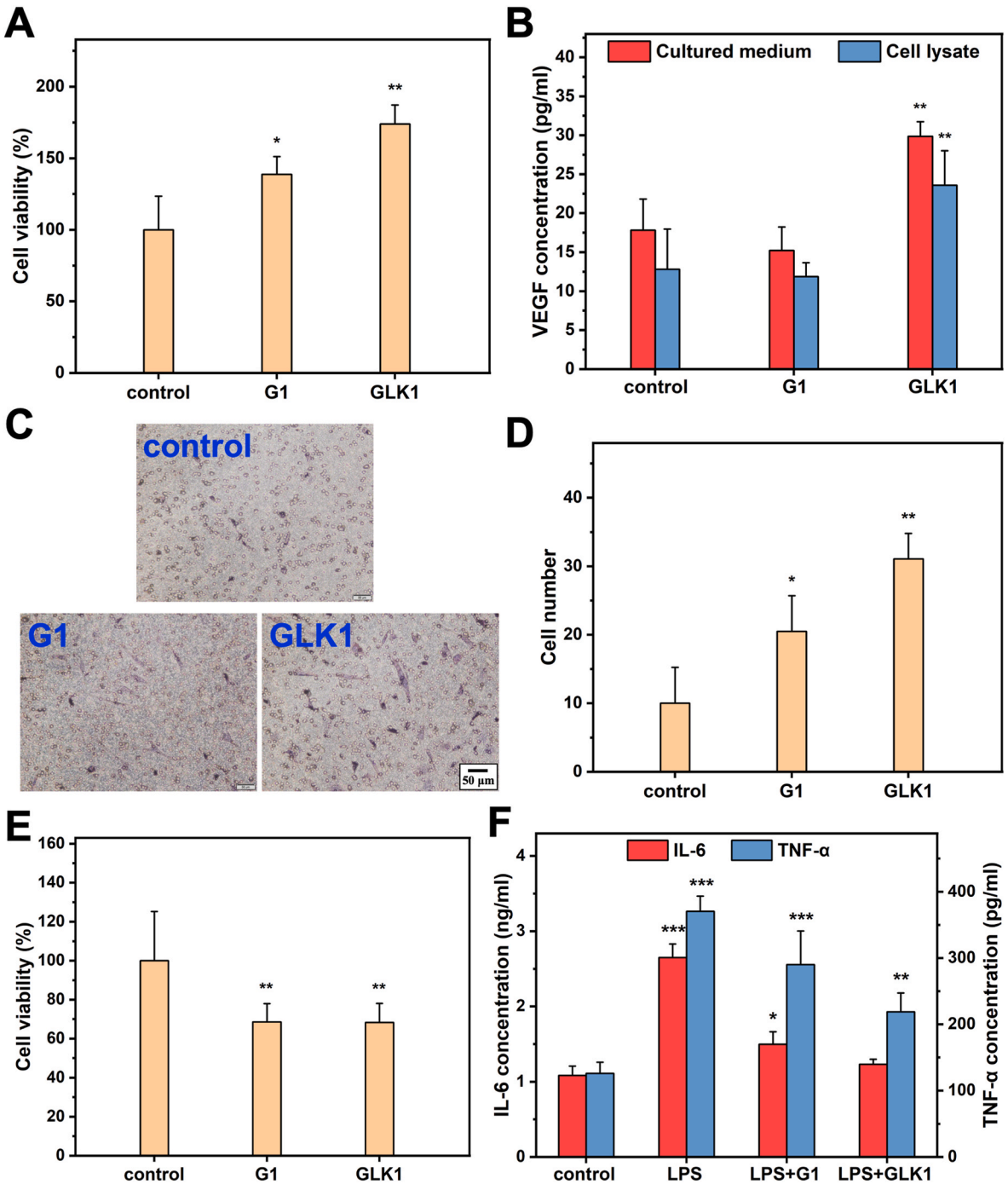

Fig. 5. Cell viability, VEGF production, and 3D migration of HUVEC cells co-cultured with GLK1 membrane. (A) Bar graphs represent cell viability of HUVEC cells following a 2-day co-culture with various membranes. (B) Bar graphs represent VEGF production in the cultured medium, and in the cell lysate of HUVEC cells following a 2-day co-culture with various membranes. Cell migration quantified by hematoxylin and eosin (HE) staining (C). The quantitative comparison of cell numbers attracted by the G1 and GLK1 membranes is shown in (D). Bar graphs represent cell viability (E), IL-6 production and TNF-α production (F) of RAW 264.7 cells treated with 1 μg/ml LPS and following a 2-day co-culture with various membranes. Asterisks indicate statistically significant differences (*$p < 0.05$; **$p < 0.01$; ***$p < 0.001$) as compared with control group.

degree of cell adhesion (Fig. 4C). By contrast, L929 cells showed improved spreading and adhesion to the G1 membrane (Fig. 4C). Cells cultured with GLK1 showed extensive spreading and better adhesion (Fig. 4C). SEM analysis of L929 cell cultures revealed that the G1 and GLK1 membranes supported cell adhesion, thus promoting the growth of densely populated cells.

3.4.2. GLK1 membrane promoted the penetration of L929 cells

Fig. 4D and E shows photographs of immunohistochemical staining conducted on L929 cells cultured on G1 and GLK1 membranes and a quantitative comparison between them. Upon seeding onto the membranes, L929 cells were counterstained with DAPI for precise quantitative analysis (shown in blue). Interestingly, L929 cells exhibited a broader distribution in terms of depth (ranging from 2 to 10 μm) within the GLK1 membranes, whereas their growth within the G1 membranes

was confined to depths of 4–8 μm (Fig. 4E). The more comprehensive range of depths observed in the GLK1 membranes suggests that the cells favored this environment, thereby indicating a potentially more conducive cell–substrate interaction and enhanced growth.

3.4.3. GLK1 membrane accelerated HUVEC proliferation

Following a 2-d co-culture period with G1 and GLK1 membranes, the proliferation rate of HUVECs was evaluated using the MTT assay. The proliferation of HUVECs cultured with G1 and GLK1 membranes exhibited a 36.8 % and 73.7 % increase, respectively, compared with that in the control group (Fig. 5A). These results indicate that the G1 and GLK1 membranes promoted the proliferation of HUVECs.

3.4.4. GLK1 membrane increased vascular endothelial growth factor (VEGF) production in HUVECs

V The VEGF is crucial in promoting the proliferation of vascular endothelial cells. Consequently, the VEGF levels were assessed in the culture medium and lysates of HUVECs (Fig. 5B) using an ELISA kit. The VEGF production in the medium and cell lysates increased significantly by 67.6 % and 84.1 %, respectively, compared with that in the control group. These findings indicate that the release of LK from the GLK1 membrane promoted the proliferation of, and enhanced VEGF production in, HUVECs.

3.4.5. GLK1 membrane promoted the three-dimensional (3D) migration of HUVECs

A Transwell migration assay was employed to evaluate the vertical migration of HUVECs; this technique serves as an in-vitro method to assess the chemotactic capability of substances. HUVECs were placed in the upper compartment and allowed to migrate through the pores of the membrane into the lower compartment, where G1 and GLK1 membranes were present. The number of cells that successfully migrated to the lower side was quantified using hematoxylin and eosin (HE) staining (Fig. 5C). The G1 and GLK1 membranes exhibited a higher degree of attraction for the migrated cells in the lower compartment than the control samples. The levels of GLK1 membranes increased significantly by 210 % and 47.6 % in the migrated cells compared with the levels of the control and G1 membranes, respectively. These findings indicate that the addition of LK enhanced the chemotactic attraction of HUVECs, as evidenced by the increased migration ability observed for the GLK1 membrane.

3.4.6. GLK1 attenuated LPS-induced inflammation in-vitro

The co-culture of RAW 264.7 macrophages with G1 and GLK1 membranes yielded noteworthy findings regarding cell viability. Fig. 5D illustrates a significant decrease in cell viability (by 30 %), thus highlighting the effect of these membranes on the health of the RAW 264.7 macrophage. Furthermore, we evaluated the anti-inflammatory potential of these membranes using cytokine ELISAs on LPS-stimulated RAW 264.7 macrophages. The results showed the stimulatory anti-inflammatory effects of the G1 and GLK1 membranes. Specifically, treatment with G1 membranes substantially reduced IL-6 production by 43.8 %, as shown in Fig. 5E. Meanwhile, the GLK1 membranes demonstrated even greater efficacy, reducing IL-6 production by 53.5 %. These findings provide compelling evidence for the anti-inflammatory properties of both the G1 and GLK1 membranes.

In addition to IL-6, the production of TNF-α, which is another pro-inflammatory cytokine, was examined. The result shows that the G1 membranes decreased TNF-α production by 21.6 %, whereas the GLK1 membranes reduced TNF-α production to a greater extent (40.9 %). These data, as presented in Fig. 5E, underscore the potent anti-inflammatory characteristics of the GLK1 membrane in attenuating LPS-induced inflammation in RAW 264.7 macrophages. Additionally, these results indicate that both the G1 and GLK1 membranes possess remarkable anti-inflammatory properties. The GLK1 membrane, in particular, exhibited robust efficacy in reducing IL-6 and TNF-α production, thus suggesting its potential as a valuable therapeutic intervention in mitigating inflammatory responses.

3.5. In-vivo wound-healing ability of GLK1 in a rat model

3.5.1. GLK1 membrane promoted wound-closure rate

The wound-closure rate serves as a critical indicator for evaluating wound-healing progress. Fig. 6A presents the macroscopic appearance of wound areas that received treatments, including G1, GLK1, Comfeel®, and gauze (control). The wounds were allowed to undergo repair for 21 d. During the first week of treatment, distinct variations in wound-recovery rates were observed among the different treatment groups. A quantitative comparison of the wound-closure rates after various treatments is shown in Fig. 6B. The wounds treated with the G1 membrane exhibited a recovery rate of 61.1 %. Comparatively, the GLK1 membrane showed a slightly lower but notable recovery rate of 42.7 %. Meanwhile, the Comfeel® and gauze treatments indicated recovery rates of 32.2 % and 23.8 %, respectively. These findings suggest that the GLK1 membrane outperformed the other membranes in terms of initial wound closure.

After 14 d of treatment, the wounds treated with the G1 membrane continued to demonstrate promising progress, reaching a recovery rate of 80.7 %. Similarly, the GLK1 membrane exhibits a reasonable recovery rate of 74.1 %. By contrast, the Comfeel® and gauze treatments showed lower recovery rates of 70.1 % and 66.6 %, respectively. After the third week of treatment, the wounds treated with the G1 membrane indicated a significant recovery rate of 86.1 %. The GLK1 membrane maintained a stable recovery rate of 78.3 %. Meanwhile, the Comfeel® and gauze treatments exhibited slightly lower recovery rates of 76.6 % and 76.8 %, respectively. These findings, as presented in Fig. 6B, emphasize the superior performance of the G1 and GLK1 membranes in promoting wound closure. Notably, the GLK1 membrane treatment consistently demonstrated better recovery rates than the other treatments, thereby demonstrating its potential to serve as an effective therapeutic option for facilitating wound healing over three weeks.

3.5.2. GLK1 membrane promoted neogenesis of hair follicles

We performed HE staining to quantify neogenic hair follicles for histological examination, as illustrated in Fig. 6C. Hair follicles contribute significantly to skin regeneration, particularly wound repair. Our findings revealed that at days 14 and 21, the wound area treated with GLK1 exhibited the highest number of hair follicles, as depicted in Fig. 6D. This suggests the beneficial effect of GLK1 treatment on promoting hair follicle formation during wound healing.

3.5.3. GLK1 membrane accelerated wound recovery

Skin injuries typically cause the epidermal thickness to increase temporarily, which is primarily attributed to keratinocyte proliferation and delayed differentiation. As wound healing progresses, the epidermal thickness gradually reverts to its normal state. Histological examinations were performed using HE staining to evaluate changes in epidermal thickness. Our extensive histological analysis provided intriguing insights into the effects of different treatment groups on epidermal repair. Notably, the histological findings depicted in Fig. 6E indicate that the new epidermal thickness in the G1 and GLK1 treatment groups was thinner than that observed in the control group. This observation suggests that the G1 and GLK1 groups had progressed to the late stage of epidermal repair. Furthermore, the epidermal thickness in the GLK1 treatment group was almost restored to normal levels (55 μm) by the third week, thus signifying significant advancements in wound healing.

3.5.4. GLK1 membrane accelerated blood-vessel formation

During wound healing, angiogenic capillary sprouts emerge and swiftly organize into a microvascular network within the granulation tissue for a few days. We performed vWF staining to assess blood-vessel formation, as illustrated in Fig. 7A. Our analysis revealed a distinct

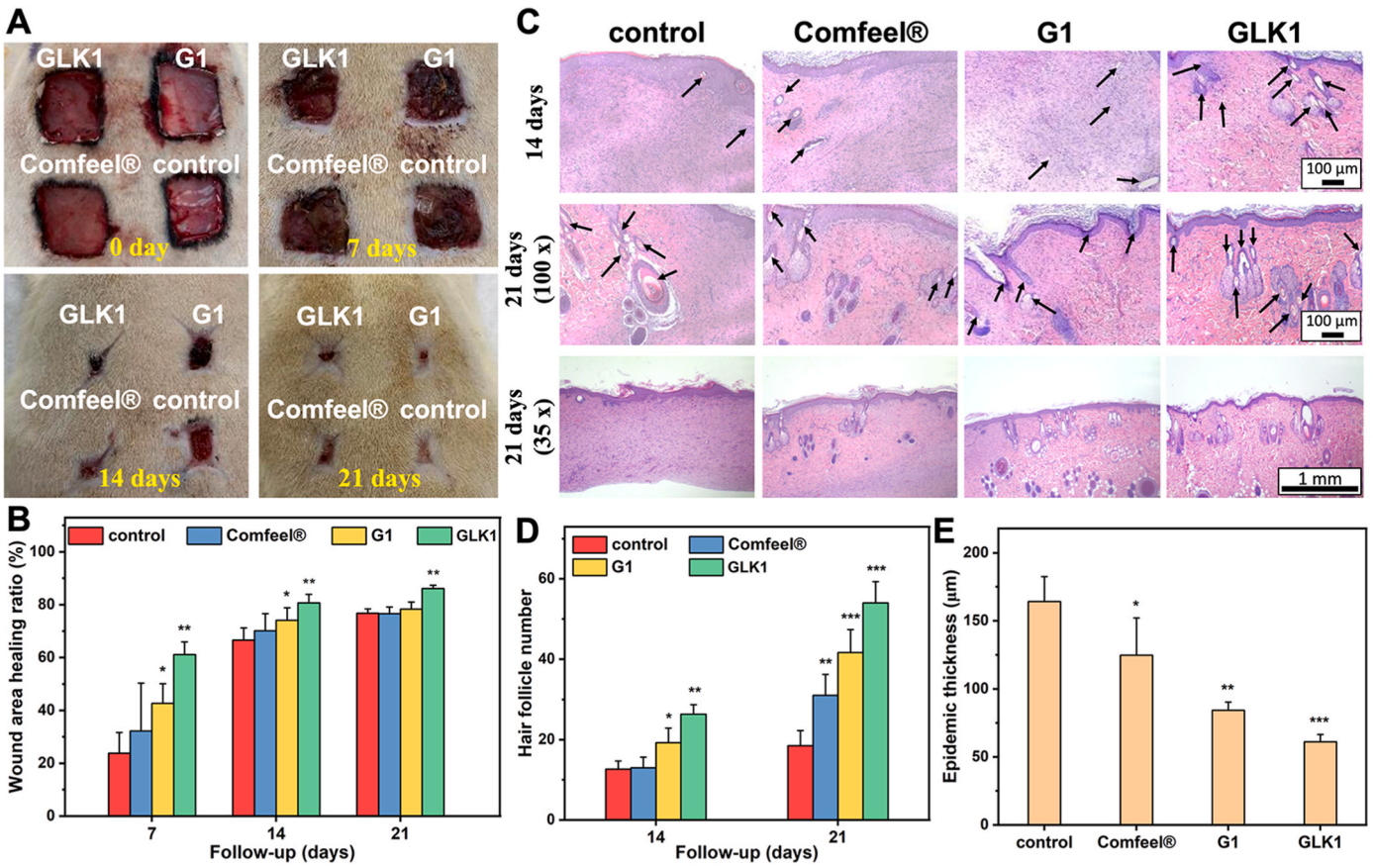

Fig. 6. Macroscopic photographs (A) and the quantitative comparison (B) of the wound areas treated with GLK membranes, gelatin membranes, Comfeel®, or gauze (control) at day 0, day 7, day 14, and day 21. GLK1 membrane promoted the neogenesis of hair follicles and epidermal repair. (C) HE staining in the wound areas treated with gauze (control), Comfeel®, gelatin membranes, or GLK membranes. The arrows indicate the hair follicles at 14 and 21 days. The marks indicate the epidemic thickness at 21 days. (D) The comparison of hair follicle number at 14 and 21 days. (E) The quantification of the epidemic thickness at 21 days. Asterisks indicate statistically significant differences (*$p < 0.05$; **$p < 0.01$; ***$p < 0.001$) as compared with control group.

pattern of blood-vessel numbers within the treated wound areas. Specifically, the GLK1 treatment group exhibited a higher number of blood vessels compared with that in the other treatment groups; during the first week of observation, a significant increase in blood vessel number (by 90.9 %) was observed in the GLK1 treatment group compared with that in the control group (Fig. 7B). These findings suggest that GLK1 treatment enhances angiogenesis by promoting the formation of new blood vessels during the early stages of wound healing.

3.5.5. GLK1 membrane increased type-I collagen levels in wound areas

Skin specimens were subjected to different membrane treatments for 7, 14, and 21 d. We employed MT staining, which stains collagen fibers blue, to assess collagen levels. Fig. 7C shows our findings, which indicate that wounds treated with G and GLK membranes exhibited higher collagen levels than those treated with other types of wound dressings on days 14 and 21. Notably, the wound area treated with the GLK membrane showed the highest production of type-I collagen. The GLK-membrane treatment increased the collagen contents significantly by 11.9 %, 149.9 %, and 345.4 % on days 7, 14, and 21, respectively, compared with those in the control group. These findings suggest that the GLK-membrane treatment promotes collagen synthesis during healing, thus potentially facilitating wound repair.

3.5.6. GLK1 membrane increased the EGF, TGF-β1, and VEGFA protein levels in wounds

Growth factors represent intracellular signaling, which coordinates complex wound-healing sequences. To investigate the effects of various treatments, we performed Western blot analysis on wounds and then examined the presence of proteins such as epidermal growth factor (EGF), transforming growth factor β1 (TGF-β1), and VEGFA. Fig. 8A illustrates the results of the Western blot analysis. The ratios of EGF protein band areas were determined and are presented in Fig. S3A. The GLK treatment resulted in a significant increase (52.03 %) in the EGF protein levels by day 14 ($p < 0.05$), compared with that in the control group. Fig. S3B highlights the effect of GLK-membrane treatment on VEGFA production in the wound area. Specifically, 136.2 % and 75.7 % increases in VEGFA production were observed on days 7 and 14, respectively, compared with that in the control group. The ratios of TGF-β1 protein band areas are depicted in Fig. S3C. After GLK treatment, the TGF-β1 protein levels increased substantially by 131.1 % ($p < 0.05$) and 112 % ($p < 0.05$) on days 7 and 14, respectively, compared with those in the control group. Furthermore, Smad-2 protein was observed on day 14 after GLK treatment (Fig. S3D). The levels of Smad-2, which is a signaling protein associated with wound healing, increased significantly on day 14 after GLK treatment.

3.5.7. In-vivo treatments with GLK membrane reduced the protein levels of the pro-inflammatory cytokines IL-6 and TNF-α in wounds

Fig. 8B shows that the IL-10 levels in the GLK-treated specimens increased by 26 % ($p < 0.05$) on day 14; this suggests the potential role of GLK in promoting the formation of a regenerative environment. As shown in Fig. 8C, treatment with the GLK membrane reduced the TNF-α levels substantially by 49 % ($p < 0.05$) and 50.1 % ($p < 0.05$) on days 7 and 14, respectively. The beneficial effects of GLK treatment were further supported by the quantification of the anti-inflammatory cytokine IL-10 using an ELISA, which is known to facilitate tissue

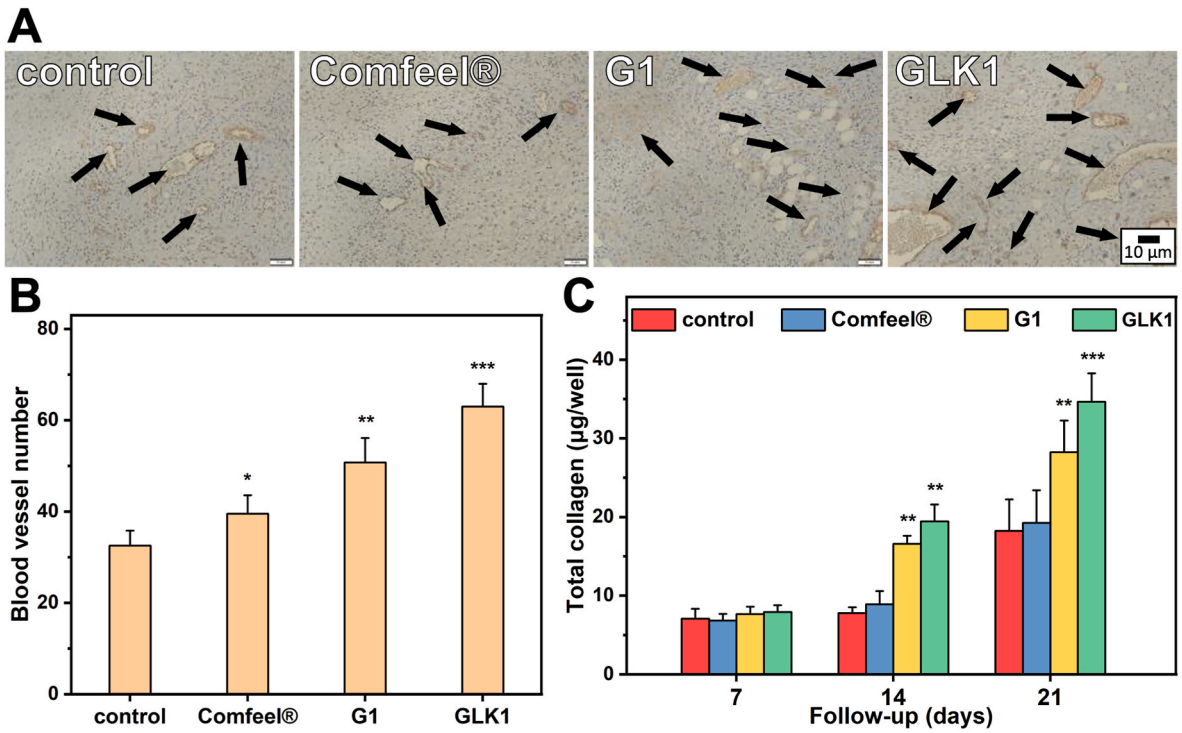

Fig. 7. (A) vWF stain of wound areas treated with gauze (control), Comfeel®, gelatin membranes, or GLK membranes at week 1, 200X. (B) The bar graphs represent the quantitative analysis of blood vessel numbers at 7 days. (C) The total collagen production in the wound. Asterisks indicate statistically significant differences (*$p < 0.05$; **$p < 0.01$; ***$p < 0.001$) as compared with control group.

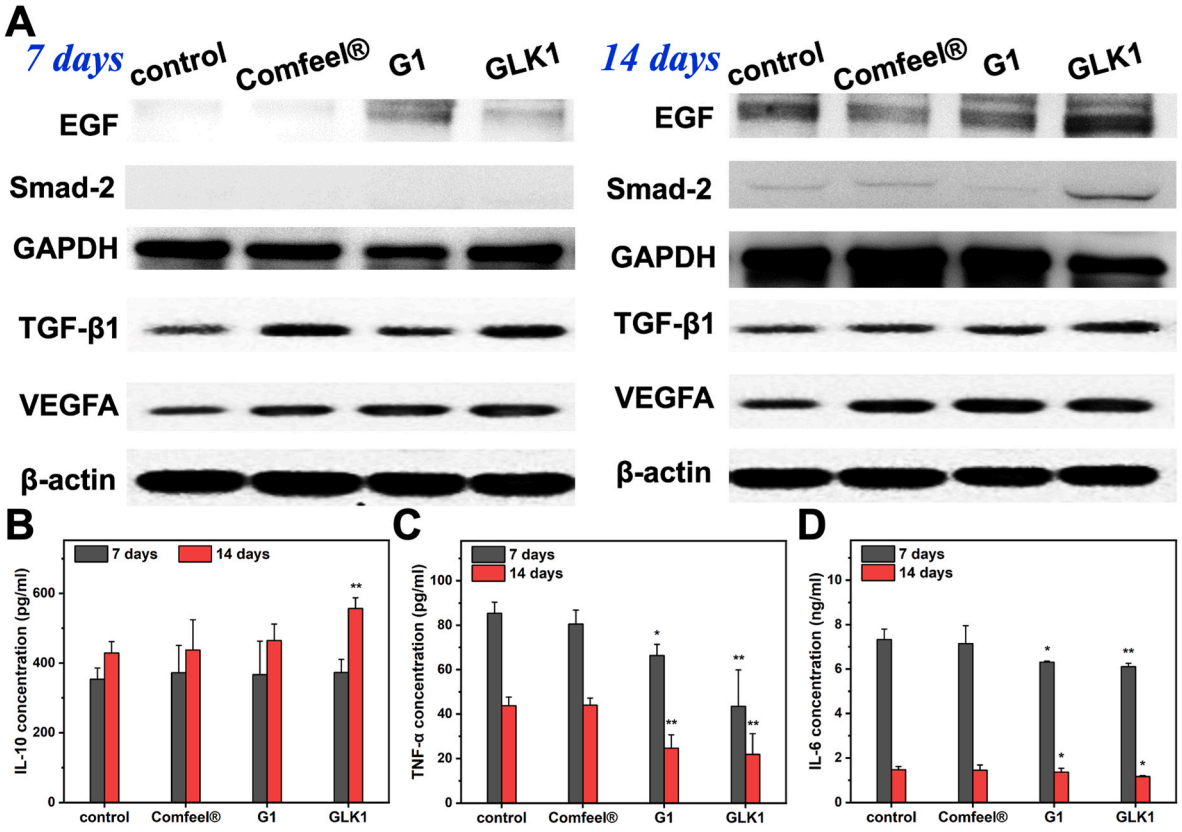

Fig. 8. (A) Western blot analysis of EGF, VEGFA, TGF-β, and Smad-2 expression in wound areas treated with gauze (control), Comfeel®, gelatin membranes, or GLK membranes at 7 and 14 days. Bar graphs represent IL-10 (B), TNF-α (C), and IL-6 production (D) in the wound areas that were treated with gauze (control), Comfeel®, gelatin membranes, or GLK membranes at 7 and 14 days. Asterisks indicate statistically significant differences (*$p < 0.05$; **$p < 0.01$) as compared with control group.

regeneration by regulating the inflammatory response. Furthermore, the application of G and GLK membranes to wounds significantly reduced the levels of the pro-inflammatory cytokine IL-6 (Fig. 8D): on day 7, the IL-6 levels decreased by 14 % and 14.5 % ($p < 0.05$), respectively, and on day 14, the levels decreased by 7.5 % and 12.5 % ($p < 0.05$), respectively.

As previously reported [27], the observed enhancements in angiogenesis, collagen production, and growth-factor stimulation may be attributed to several interconnected mechanisms. LK can accelerate hydroxyproline synthesis and TGF-β secretion, which are vital to collagen synthesis, angiogenesis, and fibroblast proliferation. Additionally, LK facilitates the removal of necrotic tissues and foreign bodies by promoting the production of IL-6, white-blood cells, and platelets. This activity likely enhances the local immunity, reduces the risk of infection, and creates a conducive environment for wound repair and regeneration.

4. Discussion

The swiftness and efficacy of skin wound healing are crucial for expediting recovery and minimizing potential complications. Dressing is typically applied to wounds to shield them from further harm, create a moist environment that fosters healing, and manage the risk of infection. Nanofiber wound dressings offer several advantages over conventional wound dressings. In particular, they possess a high surface-area-to-volume ratio, exhibit a highly porous structure, and can be customized to possess specific attributes, such as antimicrobial properties or the ability to release growth factors that facilitate healing [28,29]. In the present study, we systematically evaluated the optimum concentration of LK and the ideal parameters for electrospinning to develop a GLK membrane with the highest medical efficacy. Moreover, we assessed the bioactive effects of GLK membranes on wound healing using both in-vitro and in-vivo rat models.

To determine the optimal concentration of LK, various assays were conducted to assess its effects on the proliferation and 2D migration ability of cells and anti-inflammatory properties. The results indicated that a low LK concentration range (0.1–1 μg) stimulated the proliferation of L929 cells and HUVECs, thus enhancing tube formation. Angiogenesis, i.e., the formation of new blood vessels, is crucial for delivering oxygen and nutrients to the site of injury and facilitating tissue regeneration [30]. Earthworm extracts have been shown to promote burn wound healing through angiogenesis and endothelium regeneration [5]. In this study, we provide the first evidence that LK, which is a component of earthworm extract, promotes proliferation and angiogenesis in HUVECs.

LK concentrations of 0.1 and 1 μg/mL were evaluated in these assays. Based on the findings, 0.1 μg/mL was identified as the optimal concentration for subsequent investigations. Previous studies have highlighted the benefits of low LK concentrations (<1 μg) in promoting skin wound healing and increasing the viability and mobility of osteoblasts [31].

Gelatin nanofibers are promising as a drug-delivery system, primarily owing to their desirable properties, such as biocompatibility, biodegradability, and customizable characteristics. These nanofibers can be customized to regulate drug-release kinetics, thereby enabling sustained or targeted delivery. Once applied to the wound site, GLK nanofibers initially serve as a supportive matrix for skin regeneration by facilitating cellular attachment and tissue repair. Over time, GLK is gradually degraded and absorbed in the wound site for healing. Specific parameters were controlled during electrospinning to achieve gelatin nanofibers containing LK. The tip-to-collector distance was set at 10 cm to ensure an optimal setup. The electric potential applied during this process was maintained at 20 kV. Uniform nanofibers exhibiting an average fiber size of 79.3 ± 23.9 nm were successfully fabricated by maintaining a flow rate of 0.4 mL/h. This demonstrates the effectiveness of electrospinning in generating consistent and well-defined gelatin nanofibers for drug-delivery applications.

Two GLK membranes, i.e., GLK1 and GLK2, were prepared by varying the electrospinning time (1 and 2 h). The degradation profiles of both membranes indicated that they achieved satisfactory cross-linking networks. However, a longer fabrication time for GLK2 resulted in a thicker membrane and a lower cross-linking rate. GLK2 exhibited the highest swelling ratio after 12 h of soaking. The swelling and degradation properties of the nanofibers contributed significantly to the regulation of the drug-release rate. Upon immersion in an aqueous environment, the nanofibers absorbed water and swelled, thus facilitating drug diffusion (i.e., LK) from the matrix. Simultaneously, the degradation of the nanofibers, which was driven by hydrolytic or enzymatic processes, contributed to a sustained release via the gradual disintegration of the polymer matrix. These two processes operated synergistically. While the swelling phase facilitated a rapid initial release to address acute therapeutic demands, the degradation phase provided a prolonged release to maintain effective drug concentrations and support long-term biological processes such as collagen production, angiogenesis, and anti-inflammatory responses.

Nevertheless, GLK1 and GLK2 demonstrated the ability to release effective drug concentrations in the drug-releasing assays. Further in-vitro functional analyses were performed on the GLK1 and GLK2 membranes to identify the most appropriate electrospinning time for achieving the desired characteristics and performance. In our study, GLK1 and GLK2 were fabricated via electrospinning for 1 and 2 h, respectively. The shorter electrospinning duration of GLK1 may have resulted in a less robust matrix structure, which may have been insufficient to sustain the gradual increase in LK release over extended soaking periods, thus potentially causing the observed release plateau. By contrast, the longer electrospinning duration of GLK2 may have created a more stable and larger storage capacity within the matrix, thereby facilitating the prolonged and increased release of LK with an extended soaking time.

As a result of co-culturing L929 cells with GLK1 and GLK2 for 2 d, GLK1 significantly enhanced cell proliferation and enhanced the production of type-I collagen to the greatest degree. Collagen is vital to wound healing and type-I collagen is crucial for skin wound recovery [32]. The co-culture of L929 cells with GLK1 resulted in a more efficient production of type-I collagen than that observed after the co-culture with GLK2. During wound healing, the degradation of native type-I collagen is regulated by proteinases such as MMPs [33]. Among these enzymes, MMP-1 is critical in controlling inflammatory responses. Its primary function is to degrade and remodel the ECM. Although MMP-1 is essential for the proper progression of the inflammatory response, the excessive or prolonged activity of MMP-1 can have detrimental effects [34,35]. Thus, the activity of MMP-1 must be strictly regulated to prevent excessive ECM degradation, which can hinder wound healing or result in abnormal scarring [36]. After co-culturing L929 cells with GLK1, the MMP-1 production was found to have decreased by 15.2 %. This suggests that GLK1 decelerates collagen breakdown and promote wound healing by mitigating excessive MMP-1 activity. Based on the results of the type-I collagen and MMP-1 assays, GLK1 exhibited favorable properties and appeared to be more suitable for our specific approach in facilitating effective wound healing.

SEM analysis revealed that L929 cells effectively populated the G1 and GLK1 membranes. Moreover, a comparison of cell morphology under each condition indicated that fibroblast cells transitioned from a round to an elongated shape, and that the growth of filopodia and lamellipodia in L929 cells co-cultured with GLK1 was comparable to that co-cultured with G1. These results suggest that the inclusion of LK in the gelatin nanofibers did not compromise the biocompatibility but promoted cellular adhesion. Additionally, cells that were not in direct contact with the membrane surface penetrated the GLK1 membrane. Based on a 3D cell-density evaluation, the cells penetrated deep into the GLK1 membrane (Fig. 6D). This suggests that the GLK1 membrane created a favorable environment for fibroblast cell adhesion and

penetration owing to its suitable nanofiber and pore size. The composite structure of the GLK1 membrane facilitated cellular interactions and migration, thus enhancing its potential as a suitable scaffold for wound-healing applications.

Angiogenesis, which involves the formation of new blood vessels, contributes significantly to the efficient healing of wounds. Endothelial cell migration is a key aspect of angiogenesis. This migration process is strictly regulated by pro-angiogenic factors, with the VEGF being a critical regulator of endothelial cell migration. In an in-vitro assay, GLK1 effectively released LK, which promoted the proliferation of, and VEGF production in, HUVECs, thereby promoting their migration ability. Through mechanisms involving phosphatidylinositol 3-kinase and the small GTPase Rac-1, the VEGF increased EC permeability, stimulated proliferation, and promoted migration. Additionally, mitochondria-generated reactive oxygen species have been implicated in the regulation of VEGF-induced endothelial cell migration [37,38].

Inflammatory responses are intrinsic to the body's natural reaction to injury; however, excessive inflammation can impede healing. Cytokines are key in the regulation of wound healing. Pro-inflammatory cytokines, such as IL-6 and TNF-α, are essential in wound healing and can serve as inflammatory biomarkers [39,40]. Treatment with GLK1 notably attenuated LPS-induced IL-6 and TNF-α production in RAW 264.7 macrophages, as well as surpassed other treatments. These findings provide evidence for the anti-inflammatory effects of the GLK1 membrane. By modulating the levels of pro-inflammatory cytokines, GLK1 may contribute to a favorable inflammatory response and promote proper wound healing.

Based on the co-culture experiments, the GLK1 membrane might have promoted wound healing, angiogenesis, and anti-inflammatory effects. We conducted in-vivo assessments using an SD rat model with wounds to further evaluate its therapeutic effects. The results showed that applying GLK1 membranes resulted in the regeneration of hair follicles, the enhanced formation of blood vessels, increased production of type-I collagen, and accelerated wound closure in the wound area. Hair follicles are complex structures in the dermal layer of the skin that is crucial in wound healing. Upon injury, the activation and migration of epidermal stem cells from hair follicles contribute to wound re-epithelialization. Additionally, the formation of new blood vessels is vital for wound healing as it enhances blood circulation, nutrient supply, and cellular migration to the damaged area, thus ultimately promoting wound recovery. Macroscopic observations revealed that the GLK1 treatment resulted in the highest wound closure rate as compared with the control group, G1 membrane, and Comfeel® dressing.

Furthermore, at the molecular level, the GLK1 treatment increased the protein levels of EGF, TGF-β1, VEGFA, and interleukin-10 (IL-10). EGF is a crucial regulator of epithelial cell motility and affects the epithelialization rate [41]. TGF-β1 promotes angiogenesis and the migration of endothelial progenitor cells to facilitate blood supply to the wound site. Furthermore, it significantly affects the initiation of inflammation, granulation tissue formation, collagen formation, and wound contraction [42,43]. VEGF-A, which is a member of the VEGF family, stimulates angiogenesis and contributes significantly to wound closure, epidermal repair, granulation tissue formation, and the overall quality of wound healing [44]. After 14 d of treatment, only the GLK1 treatment resulted in a significant increase in the Smad-2 protein levels. Smad-2 participates in the TGF-β signaling pathway and modulates various cellular processes, including inflammation, cell migration, proliferation, extracellular matrix production, and angiogenesis. By coordinating these processes, Smad-2 promotes efficient wound repair [45,46]. The ability of IL-10 to promote regenerative healing may stem from its pleiotropic effects, which include modulating the inflammatory response and regulating the extracellular matrix, fibroblast function, and endothelial progenitor cells [47]. Molecular evidence suggests that GLK membranes release therapeutically active components that facilitate wound healing. The in-vivo assays confirmed that GLK1 treatment reduced the levels of the pro-inflammatory cytokines IL-6 and TNF-α in the wounds.

While various bioactive agents, such as vascular endothelial growth factor (VEGF) and epidermal growth factor (EGF), have been widely utilized in wound healing applications, they primarily function in the stimulation of specific cellular pathways to enhance tissue regeneration. However, LK offers a distinct advantage due to its dual functionality in both anti-inflammation and angiogenesis promotion. This unique mechanism allows LK to not only mitigate excessive inflammation during healing process, but also facilitate neovascularization, tissue oxygenation, and nutrient supply. It is generally recognized that growth factor-based therapies often require careful dosing and stability considerations. Unlike this treatment, the use of GLK nanofiber dressings for skin regeneration provides a sustained and localized therapeutic effect, making them a promising alternative to maintain stable wound management. This comparison highlights the potential of GLK as a multifunctional wound dressing material with advantages over conventional drug-based approaches. In conclusion, the GLK membrane exhibited notable wound healing effects on local wounds in rats. It accelerated wound healing, reduced inflammation-related damage, and functioned through mechanisms involving the enhancement of the secretion of EGF, TGF-β1, and VEGFs; further, it enhanced collagen production, angiogenesis, and fibroblast proliferation, ultimately promoting wound healing.

5. Conclusions

In the present study, we investigated the potential of gelatin nanofiber wound dressings loaded with LK to enhance wound healing. GLK membranes exhibited favorable characteristics such as controlled release of LK, stimulation of cell proliferation, augmentation of collagen production, promotion of angiogenesis, and anti-inflammatory effects. Among the different electrospinning times tested, the GLK1 membrane fabricated under a 1-h electrospinning duration demonstrated optimal results in terms of cell proliferation, collagen production, and inhibition of MMP-1 activity. Additionally, it exhibited excellent biocompatibility by facilitating fibroblast-cell adhesion and penetration. In-vitro experiments confirmed the release of LK by GLK1, which promoted VEGF production and endothelial cell migration. Additionally, GLK1 demonstrated anti-inflammatory effects by reducing the levels of IL-6 and TNF-α in macrophages. Based on an in-vivo rat model, treatment with GLK1 resulted in accelerated wound closure, the neogenesis of hair follicles, the formation of blood vessels, and increased levels of EGF, TGF-β1, VEGFA, IL-10, and Smad-2 proteins associated with wound healing. Beyond demonstrating the biological efficacy of GLK membranes, this study highlighted the scientific advancements and innovative fabrication strategies underlying LK-loaded nanofiber wound dressings. The use of electrospinning to control fiber morphology, drug loading, and release kinetics is a significant step forward in the design of bioactive wound dressings. By fine-tuning the electrospinning parameters, GLK membranes can achieve an optimal balance among mechanical stability, biodegradability, and therapeutic efficacy. Furthermore, the incorporation of LK into nanofibrous scaffolds presents a novel approach for integrating fibrinolytic, anti-inflammatory, and proangiogenic functions within a single wound dressing. Overall, the GLK membrane incorporating LK exhibited marked potential to serve as a bioactive dressing for enhancing wound healing, ameliorating inflammation, and promoting angiogenesis. The findings of the present study will not only contribute to the ongoing development of biomaterial-based wound dressings but also provide insights into the future translational applications of GLK membranes.

CRediT authorship contribution statement

Wen-Ling Wang: Writing – original draft, Investigation, Formal analysis. **Yi-Hui Lai:** Methodology, Data curation. **Chiung-Hua Huang:** Writing – review & editing, Validation, Conceptualization. **Jui-Yang**

Lai: Writing – review & editing, Project administration. **Chun-Hsu Yao:** Supervision, Funding acquisition, Conceptualization.

Declaration of competing interest

The authors declare that they have no known competing financial interests or personal relationships that could have appeared to influence the work reported in this paper.

Acknowledgments

This work was supported by grants CMU109-S-44, CMU110-S-13, CMU111-MF-85, and CMU112-S-02 from China Medical University; grants DMR-111-196 and DMR-112-178 from China Medical University Hospital; grants MOST109-2314-B-039-012-MY3 and NSTC113-2314-B-182-012-MY3 from National Science and Technology Council of Taiwan; grant CTU-111-P-004 from Central Taiwan University of Science and Technology; and grants OMRPD2N0011 and UERPD2P0181 from Chang Gung University.

Appendix B. Supplementary data

Supplementary data to this article can be found online at https://doi.org/10.1016/j.mtbio.2025.101713.

Data availability

Data will be made available on request.

References

[1] K.M. Lim, Skin epidermis and barrier function, Int. J. Mol. Sci. 22 (2021) 3035.
[2] A. El Ayadi, J.W. Jay, A. Prasai, Current approaches targeting the wound healing phases to attenuate fibrosis and scarring, Int. J. Mol. Sci. 21 (2020) 1105.
[3] D. Wang, Z. Ruan, R. Zhang, X. Wang, R. Wang, Z. Tang, Effect of earthworm on wound healing: a systematic review and meta-analysis, Front. Pharmacol. 12 (2021) 691742.
[4] Z.H. Deng, J.J. Yin, W. Luo, R.N. Kotian, S.S. Gao, Z.Q. Yi, W.F. Xiao, W.P. Li, Y. S. Li, The effect of earthworm extract on promoting skin wound healing, Biosci. Rep. 38 (2018) BSR20171366.
[5] M. He, W.Q. Xie, G. Cheng, W.P. Li, D.J. Yu, H.F. Jin, Z.H. Deng, Y.S. Li, The therapeutic effects of earthworm extract on deep second-degree burn wound healing, Ann. Pallliat. Med. 10 (2021) 2869–2879.
[6] M. Afshar, M. Hassanzadeh-Taheri, M. Zardast, Z. Naderi, Effect of earthworm oil on formation of collagen type III during wound healing process in BALB/c mice, Folia Med. 64 (2022) 267–274.
[7] R.G. Mustafa, A. Dr Saiqa, J. Dominguez, M. Jamil, S. Manzoor, S. Wazir, B. Shaheen, A. Parveen, R. Khan, S. Ali, N.M. Ali, F. Jalal, S.A. Raja, Therapeutic values of earthworm species extract from Azad Kashmir as anticoagulant, antibacterial, and antioxidant agents, Can. J. Infect. Dis. Med. Microbiol. 2022 (2022) 6949117.
[8] I. Dharmawati, T.G.B. Mahadewa, I.P.E. Widyadharma, Antibacterial activity of lumbricus rubellus earthworm extract against porphyromonas gingivalis as the bacterial cause of periodontitis, Open Access. Maced J. Med. Sci. 7 (2019) 1032–1036.
[9] S.K. Metkar, A. Girigoswami, R. Vijayashree, K. Girigoswami, Attenuation of subcutaneous insulin induced amyloid mass in vivo using Lumbrokinase and Serratiopeptidase, Int. J. Biol. Macromol. 163 (2020) 128–134.
[10] H. Sun, N. Ge, M. Shao, X. Cheng, Y. Li, S. Li, J. Shen, Lumbrokinase attenuates diabetic nephropathy through regulating extracellular matrix degradation in Streptozotocin-induced diabetic rats, Diabetes Res. Clin. Pract. 100 (2013) 85–95.
[11] R. Danarto, D.S. Heriyanto, M. Risan, P. Yuri, Lumbrokinase effects on pro- and anti-apoptotic gene expression in Wistar rats with testicular torsion, Res. Rep. Urol. 11 (2019) 249–254.
[12] Y.H. Wang, K.M. Chen, P.S. Chiu, S.C. Lai, H.H. Su, M.S. Jan, C.W. Lin, D.Y. Lu, Y. T. Fu, J.M. Liao, J.T. Chang, S.S. Huang, Lumbrokinase attenuates myocardial ischemia-reperfusion injury by inhibiting TLR4 signaling, J. Mol. Cell. Cardiol. 99 (2016) 113–122.
[13] Z.H. Deng, J.J. Yin, W. Luo, R.N. Kotian, S.S. Gao, Z.Q. Yi, W.F. Xiao, W.P. Li, Y. S. Li, The effect of earthworm extract on promoting skin wound healing, Biosci. Rep. 38 (2018) BSR20171366.
[14] X. Wang, B. Ding, B. Li, Biomimetic electrospun nanofibrous structures for tissue engineering, Mater. Today 16 (2013) 229–241.
[15] M. Liu, X.P. Duan, Y.M. Li, D.P. Yang, Y.Z. Long, Electrospun nanofibers for wound healing, Mater. Sci. Eng. C-Mater. Biol. Appl. 76 (2017) 1413–1423.
[16] Y. Li, H. Xu, W. Zhao, L. Zhang, S. Wu, Electrospun robust, biodegradable, bioactive, and nanostructured sutures to accelerate the chronic wound healing, Biofabrication 17 (2025) 025006.
[17] M. Rahman, M. Kabir, K. Li, Y. Li, S. Chen, S. Wu, Electrospun zeolitic imidazole framework-8 loaded silk fibroin/polycaprolactone nanofibrous scaffolds for biomedical application, J. Mech. Behav. Biomed. Mater. 160 (2024) 106769.
[18] Q. Meng, H. Xu, Y. Li, F. Liu, H. Shao, P. Ling, S. Wu, Conjugated electrospinning toward a polycaprolactone scaffold simultaneously containing micro-/nano- fibers for potential biomedical application, J. Polym. Res. 31 (2024) 301.
[19] I. Lukin, I. Erezuma, L. Maeso, J. Zarate, M.F. Desimone, T.H. Al-Tel, A. Dolatshahi-Pirouz, G. Orive, Progress in gelatin as biomaterial for tissue engineering, Pharmaceutics 14 (2022) 1177.
[20] M.V. Giraudo, D. Di Francesco, M.C. Catoira, D. Cotella, L. Fusaro, F. Boccafoschi, Angiogenic potential in biological hydrogels, Biomedicines 8 (2020) 436.
[21] X. Zeng, Y.S. Zeng, Y.H. Ma, L.Y. Lu, B.L. Du, W. Zhang, Y. Li, W.Y. Chan, Bone marrow mesenchymal stem cells in a three-dimensional gelatin sponge scaffold attenuate inflammation, promote angiogenesis, and reduce cavity formation in experimental spinal cord injury, Cell Transplant. 20 (2011) 1881–1899.
[22] C.H. Huang, C.Y. Chi, Y.S. Chen, K.Y. Chen, P.L. Chen, C.H. Yao, Evaluation of proanthocyanidin-crosslinked electrospun gelatin nanofibers for drug delivering system, Mater. Sci. Eng. C-Mater. Biol. Appl. 32 (2012) 2476–2483.
[23] C.H. Yao, C.Y. Lee, C.H. Huang, Y.S. Chen, K.Y. Chen, Novel bilayer wound dressing based on electrospun gelatin/keratin nanofibrous mats for skin wound repair, Mater. Sci. Eng. C-Mater. Biol. Appl. 79 (2017) 533–540.
[24] C.H. Yao, K.Y. Chen, Y.S. Chen, S.J. Li, C.H. Huang, Lithospermi radix extract-containing bilayer nanofiber scaffold for promoting wound healing in a rat model, Mater. Sci. Eng. C-Mater. Biol. Appl. 96 (2019) 850–858.
[25] Y.S. Chen, J.Y. Chang, C.Y. Cheng, F.J. Tsai, C.H. Yao, B.S. Liu, An in vivo evaluation of a biodegradable genipin-cross-linked gelatin peripheral nerve guide conduit material, Biomaterials 26 (2005) 3911–3918.
[26] M.S. Agren, H. Everland, Two hydrocolloid dressings evaluated in experimental full-thickness wounds in the skin, Acta Derm. Venereol. 77 (1997) 127–131.
[27] Z.H. Deng, J.J. Yin, W. Luo, R.N. Kotian, S.S. Gao, Z.Q. Yi, W.F. Xiao, W.P. Li, Y. S. Li, The effect of earthworm extract on promoting skin wound healing, Biosci. Rep. 38 (2018) BSR20171366.
[28] I. Maliszewska, T. Czapka, Electrospun polymer nanofibers with antimicrobial activity, Polymers 14 (2022) 1661.
[29] G. Chen, Y. Lv, Immobilization and application of electrospun nanofiber scaffold-based growth factor in bone tissue engineering, Curr. Pharm. Des. 21 (2015) 1967–1978.
[30] V. Mastrullo, W. Cathery, E. Velliou, P. Madeddu, P. Campagnolo, Angiogenesis in tissue engineering: as nature intended? Front. Bioeng. Biotechnol. 8 (2020) 188.
[31] Y.T. Fu, S.Y. Sheu, Y.S. Chen, K.Y. Chen, C.H. Yao, Porous gelatin/tricalcium phosphate/genipin composites containing lumbrokinase for bone repair, Bone 78 (2015) 15–22.
[32] S.S. Mathew-Steiner, S. Roy, C.K. Sen, Collagen in wound healing, Bioeng. Basel 8 (2021) 63.
[33] K. Dragsbaek, J.S. Neergaard, H.B. Hansen, I. Byrjalsen, P. Alexandersen, S. N. Kehlet, A.C. Bay-Jensen, C. Christiansen, M.A. Karsdal, Matrix metalloproteinase mediated type I collagen degradation - an independent risk factor for mortality in women, EBioMedicine 2 (2015) 723–729.
[34] B. Fingleton, Matrix metalloproteinases as regulators of inflammatory processes, Biochim. Biophys. Acta Mol. Cell Res. 1864 (2017) 2036–2042.
[35] M. Kandhwal, T. Behl, S. Singh, N. Sharma, S. Arora, S. Bhatia, A. Al-Harrasi, M. Sachdeva, S. Bungau, Role of matrix metalloproteinase in wound healing, Am. J. Transl. Res. 14 (2022) 4391–4405.
[36] E.S. Keskin, E.R. Keskin, M.B. Ozturk, D. Cakan, The effect of MMP-1 on wound healing and scar formation, Aesthetic Plast. Surg. 45 (2021) 2973–2979.
[37] Y. Wang, Q.S. Zang, Z. Liu, Q. Wu, D. Maass, G. Dulan, P.W. Shaul, L. Melito, D. E. Frantz, J.A. Kilgore, N.S. Williams, L.S. Terada, F.E. Nwariaku, Regulation of VEGF-induced endothelial cell migration by mitochondrial reactive oxygen species, Am. J. Physiol. Cell Physiol. 301 (2011) C695–C704.
[38] S. Wang, X. Li, M. Parra, E. Verdin, R. Bassel-Duby, E.N. Olson, Control of endothelial cell proliferation and migration by VEGF signaling to histone deacetylase 7, Proc. Natl. Acad. Sci. U. S. A 105 (2008) 7738–7743.
[39] J. Scheller, A. Chalaris, D. Schmidt-Arras, S. Rose-John, The pro- and anti-inflammatory properties of the cytokine interleukin-6, Biochim. Biophys. Acta 1813 (2011) 878–888.
[40] T. Xiao, Z. Yan, S. Xiao, Y. Xia, Pro-inflammatory cytokines regulate epidermal stem cells in wound epithelialization, Stem Cell Res. Ther. 11 (2020) 232.
[41] R.J. Bodnar, Epidermal growth factor and epidermal growth factor receptor: the Yin and Yang in the treatment of cutaneous wounds and cancer, Adv. Wound Care 2 (2013) 24–29.
[42] J.W. Penn, A.O. Grobbelaar, K.J. Rolfe, The role of the TGF-beta family in wound healing, burns and scarring: a review, Int. J. Burns Trauma 2 (2012) 18–28.
[43] X.J. Wang, G. Han, P. Owens, Y. Siddiqui, A.G. Li, Role of TGF beta-mediated inflammation in cutaneous wound healing, J. Invest. Dermatol. Symp. Proc. 11 (2006) 112–117.
[44] S.A. Eming, T. Krieg, Molecular mechanisms of VEGF-A action during tissue repair, J. Invest. Dermatol. Symp. Proc. 11 (2006) 79–86.

[45] R. Hosokawa, M.M. Urata, Y. Ito, P. Bringas Jr., Y. Chai, Functional significance of Smad2 in regulating basal keratinocyte migration during wound healing, J. Invest. Dermatol. 125 (2005) 1302–1309.

[46] D. Mokoena, S.S. Dhilip Kumar, N.N. Houreld, H. Abrahamse, Role of photobiomodulation on the activation of the Smad pathway via TGF-beta in wound healing, J. Photochem. Photobiol. B Biol. 189 (2018) 138–144.

[47] A. King, S. Balaji, L.D. Le, T.M. Crombleholme, S.G. Keswani, Regenerative wound healing: the role of interleukin-10, Adv. Wound Care 3 (2014) 315–323.